



# On the grinding effects of high-silicon iron tailings

Yun-hong Cheng<sup>1</sup> · Bai-qiang Tong<sup>1</sup> · Xiao-hui Sun<sup>1</sup> · Jing-yu Zhang<sup>1</sup>

Received: 26 February 2022 / Accepted: 16 May 2022 / Published online: 27 May 2022  
© The Author(s), under exclusive licence to Springer-Verlag GmbH Germany, part of Springer Nature 2022

## Abstract

The main chemical component of high-silicon iron tailings (HSITs) is  $\text{SiO}_2$ ; HSITs also include some oxides such as  $\text{Al}_2\text{O}_3$  and  $\text{CaO}$ . Mechanical activation can reduce the particle size of HSITs and enhance their pozzolanic activity such that they can be used as a type of mineral admixture for cement-based materials (CBMs). This study aims to investigate the mechanical activation (ultrafine grinding) effects of HSITs, including physical and crystallization structure effects. The particle distribution, specific surface area, density, and solubility of HSITs were tested using laser particle size analysis and other routine physical testing methods. Their crystal structures were analyzed using X-ray diffraction (XRD), Fourier transform infrared spectroscopy (FTIR), and differential scanning calorimetry-thermogravimetry (DSC-TG). Grinding reduced the particle size of HSIT particles and increased their specific surface area, wherein the minimum D50 was 5.75  $\mu\text{m}$ , the maximum specific surface area was 7608  $\text{m}^2/\text{kg}$ , and the corresponding grinding time was 3.5 h. With an increase in grinding time, the solubility showed an increasing trend; however, the density showed a decreasing trend. The change was fast before 3.5 h or 4 h and then slowed down, but the final solubility was still higher than its initial level, while the final density was still lower than its initial level. Grinding reduced the degree of crystallization of the minerals in HSITs and increased the microscopic strain and disorder of its crystal structure. These changes were significant for a grinding time of 0–3.5 h, after which the changes tended to be slow. The symmetry and integrity of the  $\text{SiO}_2$  structure decreased with grinding. The activity index of the HSIT powder was higher than 0.6. Ultrafine grinding improves the particle size distribution of HSITs and reduces the crystallinity of their main minerals, which in turn increases their chemical reactivity. It can be said that ultra-finely ground HSIT powder is pozzolanic and can be used as a mineral admixture for CBMs, and its grinding limit can be inferred to be 3.5 h.

**Keywords** High-silicon iron tailings · Grinding · Particle size distribution · Crystallinity

## Abbreviations

HSITs	high-silicon iron tailings
CBMs	cement-based materials
DPI	diffraction peak intensity
FWHM	full width at half maximum
XRD	X-ray diffraction
FTIR	Fourier transform infrared spectroscopy
DSC-TG	differential scanning calorimetry-thermogravimetry

## Introduction

China is rich in iron ore resources, and the exploitation of iron ore has greatly contributed to the development of the national economy and the improvement of living standards. However, the large amounts of iron tailings produced in the beneficiation process have caused significant environmental problems. The inventory of iron tailings has reached 5000 million tons in the country and is steadily growing at more than 300 million tons per year (Lv et al. 2021). Its recycling rate, however, is less than 10% (Zhang et al. 2020a; Wu and Liu 2018; Zhang et al. 2020b).

High-silicon iron tailings (HSITs) are a major type of iron tailings. HSITs are mainly composed of  $\text{SiO}_2$ ; it can also include oxides such as  $\text{Al}_2\text{O}_3$  and  $\text{CaO}$ . The chemical constituents of HSITs are similar to those of pozzolanic materials; therefore, HSITs have great potential as mineral admixtures for cement-based materials (CBMs). However, HSITs are inert and do not exhibit pozzolanic activity at room temperature

Responsible Editor: George Z. Kyzas

✉ Yun-hong Cheng  
cyh\_neu@163.com

<sup>1</sup> Northeastern University, Shenyang 110819, China

(Yao et al. 2020; Wu et al. 2020); therefore, a certain activation treatment is required before they can be used as mineral admixtures for CBMs.

The main activation methods for tailings include mechanical, chemical, thermal, and compound activation (Saedi et al. 2020; Li and Hitch 2017). Mechanical activation (Wang et al. 2022; Zhang et al. 2022a; Li and Hitch 2017; Allahverdi and Mahinroosta 2013; Sajedi 2012) involves applying mechanical energy to the tailings, such as through grinding; this changes its physical and chemical properties, such as particle size, specific surface area, density, and crystalline state. Chemical activation (Akinyemi et al. 2022; Yu et al. 2022; Zhang et al. 2022b; Perumal et al. 2021; Kiventera et al. 2018) is the use of an organic or inorganic reagent to stimulate the activity of the tailings. After adding a certain amount of chemical activator, the silicon oxygen tetrahedron or aluminum oxygen tetrahedron in the tailings is decomposed and can then be repolymerized in a suitable solution environment to form a new structure. Thermal activation (de Magalhaes et al. 2020; Soury et al. 2015; Ferreira et al. 2013) involves using a high-temperature calcining method to change the structure of minerals or allow minerals to undergo phase transformation, thereby changing their physical and chemical properties. Compound activation (Chen et al. 2022a, 2022b; Jiang et al. 2022; Vargas and Lopez 2018) is usually a combination of two activation methods, such as thermochemical activation. Among these methods, the mechanical activation method is relatively simple and easy to use because it does not require a high temperature or any chemical activator during the operation process; therefore, this method is widely used in the activation treatment of HSITs.

CBMs, such as concrete, are globally used as a construction material. However, the large-scale use of such materials causes environmental problems. For example, the production of cement consumes natural resources and emits CO<sub>2</sub> (Chen et al. 2022a, 2022b). A large number of researchers have made great efforts toward reducing carbon emissions among which replacing part of the cement with mineral admixtures to prepare CBMs is an effective method (Tushar et al. 2022). Traditional mineral admixtures primarily include fly ash and granulated blast furnace slag powder (Lv et al. 2022); the use of these materials decreases the amount of cement in CBMs and reduces the environmental impact of cement production (Vargas and Lopez 2018). Owing to the increasing use of mineral admixtures, the development of new types of mineral admixtures is crucial for the sustainable development of CBMs (Yao et al. 2020). Studies (Cheng et al. 2022; Cheng et al. 2020; Cheng et al. 2016; Han et al. 2022; Han et al. 2020) have shown that when HSITs are mechanically ground, their

particle size reduces and their pozzolanic activity increases, making it possible for them to be used as a mineral admixture in CBMs.

However, based on the existing literature, research on HSITs as a new mineral admixture, is limited, particularly regarding its ultrafine grinding effect. To further develop and utilize this mineral admixture, it is important to study its grinding effect and related mechanisms. This study aims to systematically investigate the mechanical activation (grinding) of HSITs to evaluate the effect on its physical and crystallization structure. The results are of great significance for revealing the mechanism of mechanical activation and providing a theoretical basis for further research on mineral admixtures made using HSITs.

## Properties and grinding methods of HSITs

HSITs were obtained from a tailing pond in Hebei Province, China. The main chemical constituents are SiO<sub>2</sub>, followed by Fe<sub>2</sub>O<sub>3</sub>, MgO, CaO, and Al<sub>2</sub>O<sub>3</sub> (Table 1); the main mineral constituent is quartz (Fig. 1); the shape of the particles is irregular, and the surface of the particles is uneven and angular (Fig. 2); the particle size is mainly distributed in the range of 50–150 μm (Fig. 3), and the D50 and specific surface area are 132 μm and 122 m<sup>2</sup>/kg, respectively.

In this study, grinding was used as the mechanical activation method of the HSITs. The grinding equipment was a planetary ball mill (product model XQM-4), manufactured

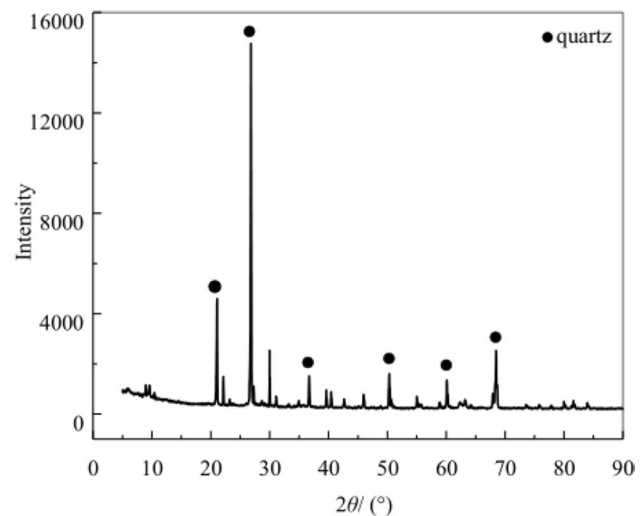
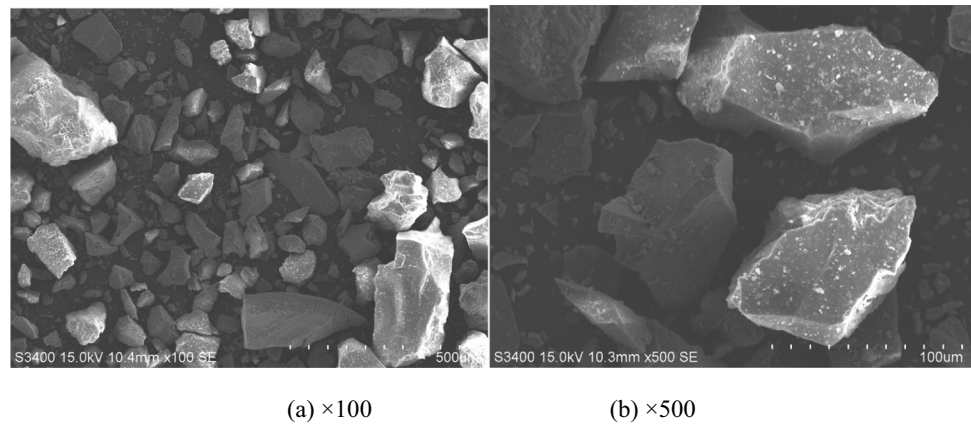


Fig. 1 XRD patterns of the HSITs

**Table 1** Main chemical constituents of the HSITs/wt%

SiO <sub>2</sub>	Fe <sub>2</sub> O <sub>3</sub>	MgO	CaO	Al <sub>2</sub> O <sub>3</sub>	AlPO <sub>3</sub>	SO <sub>3</sub>	TiO <sub>2</sub>	LOI
78.690	5.527	4.310	2.873	2.156	1.850	0.093	0.079	2.283

**Fig. 2** Particle morphology of the HSITs. **a**  $\times 100$ . **b**  $\times 500$



**Fig. 3** Particle size distribution of the HSITs. **a** Differential distribution. **b** Cumulative distribution

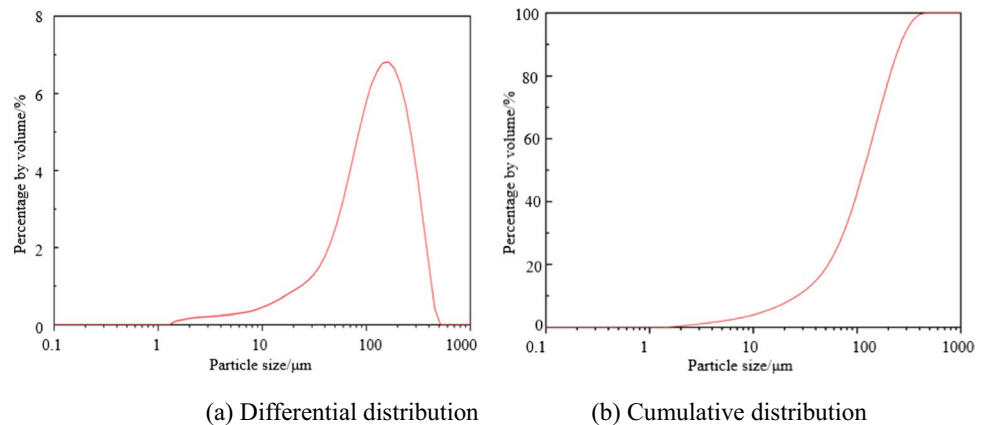


**Table 2** Main technical parameters of the planetary ball mill

Model	Power supply	Rated power/ kW	Rotation speed of the mill tank/ rpm	Total running time range/ min
XQM-4	220 V/50 Hz	0.75	70–670	1–9999

by Changsha Tianchuang Grinding Technology Co., LTD., China. The main technical parameters are listed in Table 2, and the internal structure is shown in Fig. 4.

The working principle of the mill is that the four ball milling tanks mounted on a turntable revolve with the turntable and simultaneously make planetary rotation in reverse direction on its own axis. The grinding balls and the materials in the tanks collide, shear, and rub each other to reduce the size of the material. After grinding, the minimum particle size of the materials could reach 0.1  $\mu\text{m}$ .

Repeated pre-tests were performed to obtain a higher grinding efficiency. The grinding parameters are listed in Table 3.

## Physical effects of grinding of HSITs

### Test design

#### Determination of particle size and specific surface area

The particle size and specific surface area of the HSITs were measured using a laser particle size analyzer. A laser particle size analyzer used laser diffraction technology to measure the particle size of the sample. The working principle is that when a laser beam passes through the dispersed particle sample, the particle size is accurately determined by measuring the scattered light intensity of the sample, which is used to obtain the particle size distribution diagram and specific surface area.

The laser particle size analyzer used in this study was a Mastersizer 3000, manufactured by Malvern Instruments



Fig. 4 Internal structure of the planetary ball mill

Table 3 Grinding parameters

Ball-to-material ratio (by mass)	Ratio (by mass) of balls with diameters of 15, 12, 10, 8, and 5 mm	Rotating speed/r/min
3.75:1	10:10:25:25:30 (average ball diameter 8.70 mm)	360

Ltd., UK, and the test particle size range of the equipment is 0.01–3500 μm.

**Determination of density**

The density was calculated using the pycnometer test method, which is a highly accurate method for determining the densities of powders and particles.

Table 4 D50 of HSIT particles under different grinding times

Grinding time/h	0	2	2.5	3	3.5	4	4.5	5	7
D50/μ m	132	8.29	6.90	6.06	5.75	5.86	6.44	6.55	6.75

The sample was placed into a pycnometer, the air bubbles in the pycnometer were removed at a constant temperature, the volume of water discharged from the pycnometer was measured by the sample, and the density of the sample was calculated based on the volume and mass of the sample. There were four samples in each group and the average values were calculated.

**Determination of solubility**

Under constant temperature conditions, the sample and water were put into a beaker, and the beaker was placed in a blender for 30 min and then allowed to stand for a while. The composition of the upper solution was analyzed to test the solubility at this temperature.

We averaged the value of 9 samples in each group.

**Results and discussion**

**Particle size and specific surface area**

The particle size varied with grinding time, as shown in Table 4. Table 4 indicates that after grinding for 0–3.5 h, the D50 exhibits a rapid downward trend from 132 to 5.75 μm at a decreasing rate of 95.64%. This is the result of rapid particle breakage caused by initial grinding (Wang et al. 2022). After grinding for 3.5–5 h, the D50 increases from 5.75 to 6.55 μm at a growth rate of 13.91%. This is due to particle aggregation (Perumal et al. 2020; Alex et al. 2014; Sajedi 2012) caused by extra surface energy (Sajedi 2012; Sajedi and Razak 2011). After grinding for 5–7 h, the D50 changes from 6.55 to 6.75 μm at a change rate of 3.1%. The fluctuation range is small, during which the HSIT particles enter the dynamic equilibrium stage of crushing, refining, and agglomeration, that is, reaching the grinding limit (Perumal et al. 2020).

Table 4 records that the particle size is smallest after grinding for 3.5 h. Figure 5 shows that the curve of particle size distribution shifts significantly to the left and widens (Fig. 5a), indicating that the particle size decreases and the particle distribution becomes more uniform after grinding.

The changes in the specific surface area with grinding time are listed in Table 5. As listed in Table 5, the specific surface area increased rapidly from 122 to 7608 m<sup>2</sup>/kg during grinding for 0–3.5 h. An increase of 61.36 times that

**Fig. 5** Particle size distribution of HSITs after grinding for 3.5 h. **a** Differential distribution. **b** Cumulative distribution

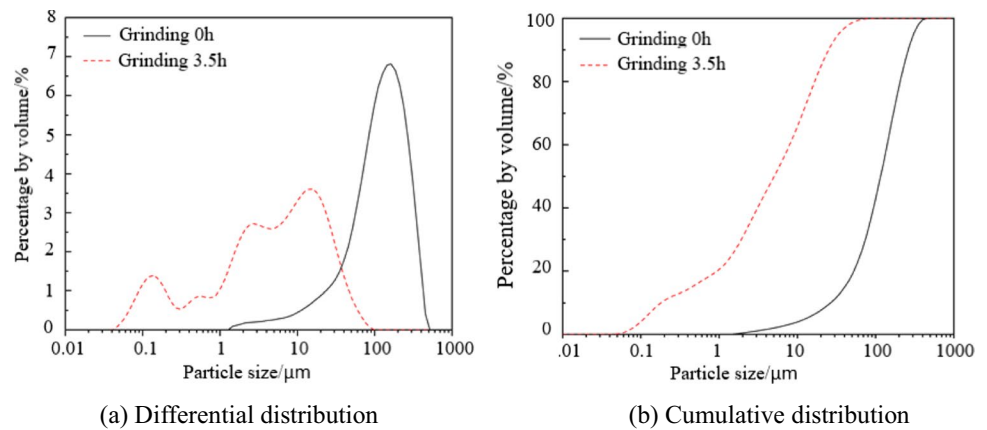


**Table 5** Specific surface area of HSIT particles under different grinding times

Grinding time/h	0	2	2.5	3	3.5	4	4.5	5	7
Specific surface area/m <sup>2</sup> /kg	122	5297	5824	7277	7608	7258	6769	6487	6604

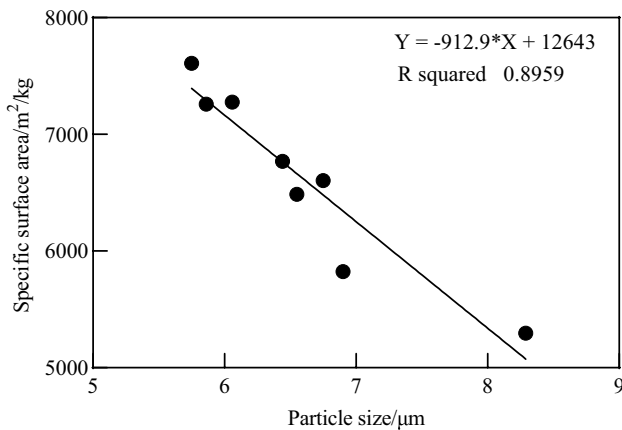


**Fig. 6** Relationship between particle size and specific surface area of HSITs

may be attributed to the combined effect of grinding-induced particle breakage, internal microcracks, and pores (Wang et al. 2022). During grinding 3.5–5 h, the specific surface area decreased from 7608 to 6487 m<sup>2</sup>/kg at a decreasing rate of 14.73%. The specific surface area changes from 6487 to 6604 m<sup>2</sup>/kg with a small change rate of 1.8% during grinding for 5–7 h. The reduction of specific surface area is because the particle aggregation rate is higher than the breakage rate. The decrease tends to be stable after grinding reaches a certain level (Li et al. 2022). Studies have shown that the variation in specific surface area with grinding time is negatively correlated with the variation in particle size (Fig. 6),

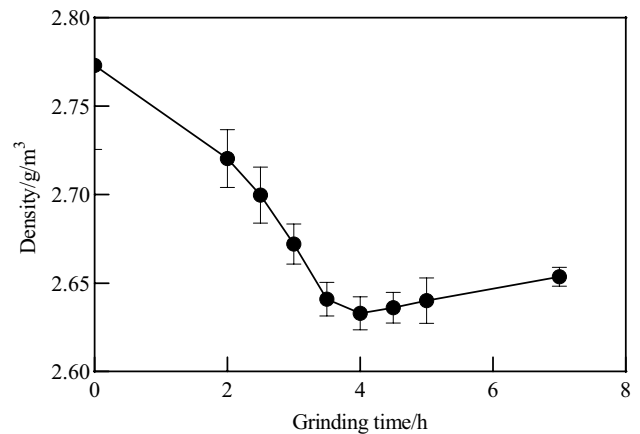


**Fig. 7** Variation in density of HSITs with grinding time (error bars indicate mean values with standard error of the mean, which were calculated using GraphPad Prism 8.3.0.)

which is similar to the relevant law obtained by Kitamura and Senna (2001).

Furthermore, based on the particle size and specific surface area, the grinding limit of the HSITs in this study can be inferred to be 3.5 h.

### Density

The variation in density with the grinding time is shown in Fig. 7. Figure 7 shows that the density exhibits a downward trend after grinding for 0–4 h, at a decrease rate of 5.05%, during which the particles are quickly broken and refined. Under a strong mechanical force, cracks or voids inside the

particles increases, or ultrafine grinding may cause an amorphous layer (Perumal et al. 2020; Kitamura and Senna 2001) on the surface of the particles, resulting in a decrease in the density. After grinding for 4–7 h, the density increased slightly at a rate of 0.80%. This is because after the grinding limit, the particles are in a dynamic balance of refinement and aggregation, during which the particles suffer from violent mechanical collision and grinding; the internal cracks or voids are continuously squeezed and welded (Sahraoui et al. 2016) resulting in an increase in the density; however, the compaction inside the particles is a physical phenomenon and will not form the tightest internal structure, so the final density is still less than the initial density:

### Solubility

Figure 8 presents the variation in solubility with grinding time. As shown in Fig. 8, the solubility showed an upward trend after grinding for 0–3.5 h, at a growth rate of 31.06%. On the one hand, with the progress of grinding, the particle size decreases, while the specific surface area increases, which expands the contact area between HSIT particles and water, leading to the rise of solubility (Tõnsuaadu et al. 2011); on the other hand, ultrafine grinding may cause the amorphization (Perumal et al. 2020; Kitamura and Senna 2001) of minerals in HSITs and the formation of an amorphous layer on the surface of the particles, thereby increasing the solubility (Chen et al. 2019). After grinding for 3.5–7 h, the solubility decreased slightly at a reduction rate of 6.74%. This was due to particle aggregation after the grinding limit that reduced the contact area between the particles and water. However, despite the occurrence of particle aggregation,

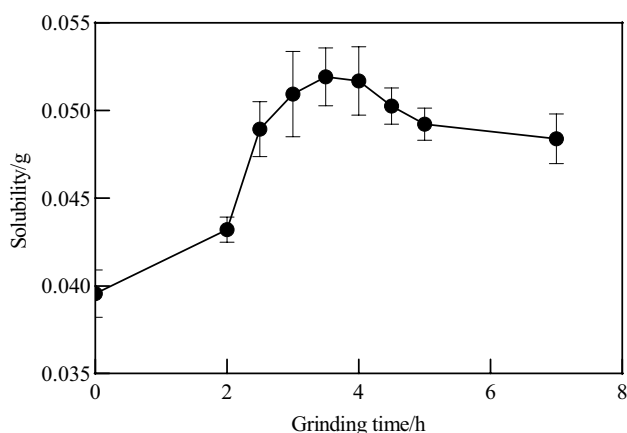


**Fig. 8** Variation in solubility of HSITs with grinding time (error bars indicate mean values with standard error of the mean, which were calculated using GraphPad Prism 8.3.0.)

the specific surface area was still larger than the initial one, and thus, the minimum solubility was higher than the initial solubility.

## Crystallization structure effects of grinding of HSITs

### Test design

#### X-ray diffraction (XRD)

XRD is a technique for analyzing the structure of materials using the diffraction effect of X-rays by crystals. When a beam of monochromatic X-rays is incident on a crystal, the X-rays scattered by different atoms interfere with each other, resulting in strong X-ray diffraction in specific directions. The orientation and intensity of the diffraction lines in space are closely related to their crystal structure.

The crystal structure changes of the main minerals in the HSITs with grinding time were analyzed using XRD. The instrument used was an X Pert Pro polycrystalline X-ray diffractometer developed by PANalytical in the Netherlands. The  $2\theta$  test range was  $0\text{--}167^\circ$ , the test accuracy was  $2\theta \pm 0.01^\circ$ , and the test data were analyzed using MDI Jade 6.0.

#### Fourier transform infrared spectroscopy (FTIR)

Infrared spectroscopy can be used to study the structure and chemical bonds of molecules as well as to characterize and identify the chemical species. A beam of infrared light having different wavelengths irradiates the molecules of the substance. Some infrared rays of specific wavelengths are absorbed to form the infrared absorption spectrum of this molecule. Each molecule has a unique infrared absorption spectrum determined by its composition and structure, which can be used for structural analysis and identification.

A Fourier infrared spectrometer (IR Affinity-1) was used to obtain more information about the crystal structures of the HSIT samples. We used an infrared spectrometer with a wavenumber range of  $7800\text{--}350\text{ cm}^{-1}$  and a resolution of  $0.5\text{--}16\text{ cm}^{-1}$ , developed by Shimadzu Corporation, Japan. Changes in the infrared spectral characteristic bands with grinding time were observed to reveal the law of chemical bonds in the grinding process.

## Differential scanning calorimetry-thermogravimetry (DSC-TG)

The DSC-TG method can accurately measure and record a series of physical and chemical phenomena such as water loss, decomposition, phase transformation, redox, and lattice destruction and reconstruction of a substance during the heating process.

DSC-TG experiments were carried out to evaluate the relationship between thermal energy and mass change of HSIT samples, in order to reveal the influence of mechanical grinding on the crystal structure and physicochemical properties of HSITs based on its thermal properties.

In the tests, the heating rate was controlled at 10 °C/min in a nitrogen environment, and a synchronous thermal analyzer (STA449F3) manufactured by NETZSCH, Germany was used.

## XRD results and analysis

### Diffraction peak intensity (DPI), full width at half maximum (FWHM), and crystallinity

The diffraction peaks of the quartz crystal faces for different grinding times are shown in Fig. 9.

As shown in Fig. 9a, the DPI of each crystal face of quartz decreased to different degrees under the action of mechanical force. Although the DPI of some crystal faces increases for 3.5–7 h, the increase was small and still lower than the initial value; on average, the DPI of each crystal face decreased by 36.06%. Figure 9 b–g show that with the grinding time, the diffraction peaks shift and exhibit a broadening trend. Similarly, the FWHM of the diffraction peak decreases for 3.5–7 h, but the reduction was small, and the diffraction peaks of each crystal face broadened by 39.35% on average.

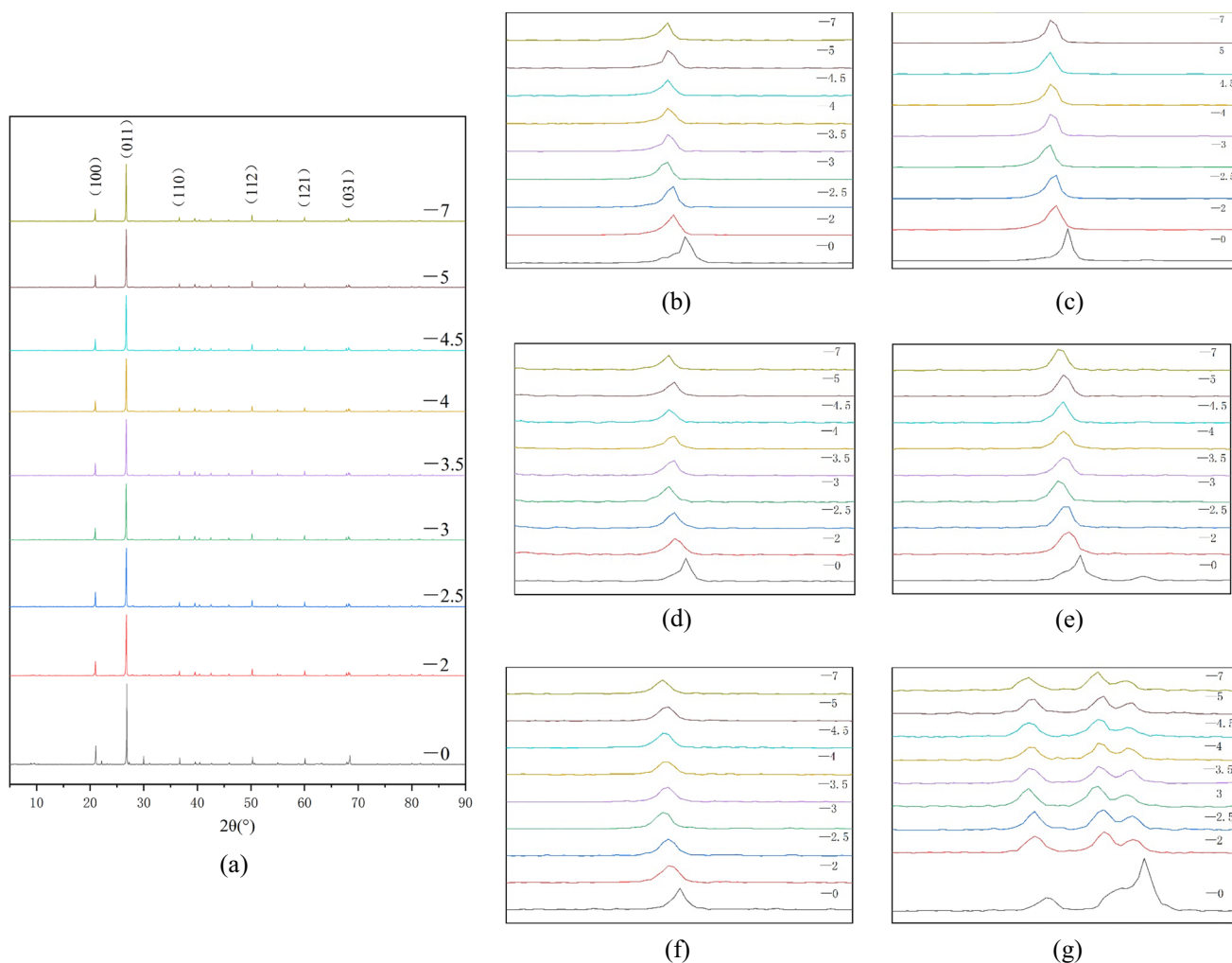


**Fig. 9** XRD patterns of quartz minerals in HSITs at different grinding times. **a** Comparison of crystal faces. **b** Crystal face (100). **c** Crystal face (011). **d** Crystal face (110). **e** Crystal face (112). **f** Crystal face (121). **g** Crystal face (031)

During the grinding process, the mechanical energy generated by cutting, compression, tension, bending, and impact is converted into unstable energy on the lattice surface, which destroys the crystal structure of the solid surface, resulting in a decrease in the DPI (Wang et al. 2022). In addition, the DPI decreases owing to the mechanical force that causes the amorphization of quartz (Kitamura and Senna 2001). With an increase in the grinding time, the degree of amorphization increases, but the diffraction peaks do not completely disappear, indicating that the amorphization is limited to the local region. This is because of the greater grinding resistance of minerals (Li et al. 2022). This can be further studied in order to adjust the grinding efficiency. The diffraction peaks shift and broaden because of the decrease in the crystal grain dimensions and the increase in the microscopic strain of quartz caused by the mechanical force (Yang et al. 2022; Alex et al. 2014). The small fluctuations in DPI and FWHM after the grinding limit may be because the particles are in an unstable high-energy state during the dynamic equilibrium process of crushing and agglomeration, causing some changes in their microstructure. This can be a topic of further research.

Crystallinity reflects the degree of crystallization. It can be inferred from the variation in the DPI and FWHM with the grinding time that the crystallinity changes correspondingly. Therefore, the crystallinity was determined based on the XRD patterns (Li et al. 2022) using MDI Jade 6.0. The results are listed in Table 6.

Table 6 records that mechanical force reduces the crystallinity, which is consistent with the results in Wang et al. (2022) and Ermolovich and Ermolovich (2016). For the period 0–3.5 h, the crystallinity dropped quickly, down by 59.33%. After 3.5–7 h, the crystallinity dropped slowly, down by 31.94%. Although the crystallinity fluctuates slightly after the grinding limit, the general trend was decreasing. This is consistent with the change law of DPI and FWHM. The reason for the decrease in crystallinity is that grinding destroys the crystal structure and forms defects (Boldyrev 2006; Wang et al. 2022); the continuous high-energy effect of grinding can cause the minerals such as quartz to transform from crystalline state to amorphous state (Zielinski et al. 1995; Chen et al. 2019).

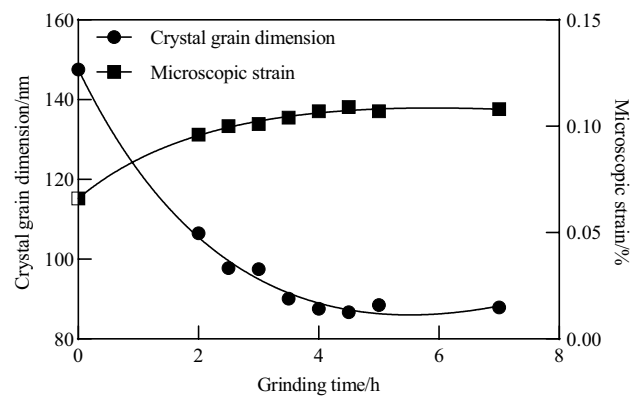


Fig. 10 Variation of crystal grain dimension and microscopic strain with grinding time

**Crystal grain dimension, microscopic strain, and Debye–Waller factor**

Furthermore, the crystal grain dimension, microscopic strain, and Debye–Waller factor were analyzed using MDI Jade 6.0.

The changes in crystal grain dimensions and microscopic strain are plotted in Fig. 10. Figure 10 shows that the crystal grain dimension decreased, whereas the microscopic strain increased with grinding time. The two have an inverted relationship, and both have a larger range of change for the period 0–3.5 h and a smaller range of change for the period 3.5–7 h.

The decrease in crystal grain dimensions and increase in microscopic strain have confirmed the existence of microcrystalline boundaries and defects (Alex et al. 2014). Under the action of mechanical force, when the internal stress in the HSIT particles is greater than the ultimate shear stress of lattice sliding, the lattice slips and fragments. The mechanical grinding energy is primarily converted into microstructural strain and deformation of the particles (Wang et al. 2022), resulting in a decrease in the crystal grain dimension and corresponding increase in the microscopic strain. A decrease in the crystal grain dimension causes the grain boundary to increase, leading to an increase in the microscopic strain because part of the energy is stored in the grain boundaries (Sasikumar et al. 2009). Furthermore, the variation law of the crystal grain dimension and microscopic strain strongly supports the broadening of the diffraction peaks of each crystal face (Ermolovich and Ermolovich 2016; Yang et al. 2022) of quartz, as shown in Fig. 9.

**Table 6** Crystallinity under different grinding times

Grinding time/h	0	2	2.5	3	3.5	4	4.5	5	7
Crystallinity/%	100	56.13	50.87	43.15	40.67	40.74	34.12	31.47	27.68



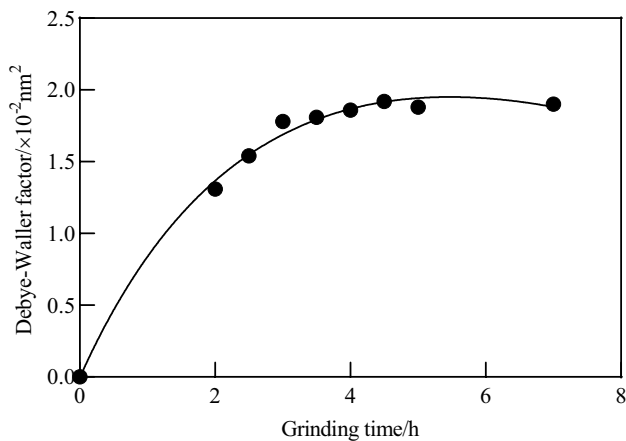


**Fig. 11** Variation in Debye–Waller factor with grinding time

The Debye–Waller factor exhibits an upward trend with grinding time, as shown in Fig. 11.

The Debye–Waller factor characterizes the dynamic characteristics of the crystal lattice (Purushotham and Krishna 2015), reflects the vibration amplitude of the atom, and corresponds to the disorder of the structure. As the grinding progresses, mechanical energy is continuously stored inside the crystal grains such that the internal energy increases,

which leads to aggravated lattice vibration and an increase in the degree of disorder (Pourghahramani et al. 2008), thereby increasing the Debye–Waller factor.

In summary, the variation in the Debye–Waller factor with grinding time has a positive relationship with microscopic strain and an inverse relationship with crystal grain dimension, which is consistent with the research results of Purushotham and Gopi (2014).

### FTIR results and analysis

The infrared spectra of the HSIT samples with different grinding times are shown in Fig. 12.

Absorption bands in the FTIR spectra of microcrystalline solids are often assigned to vibrations of ions in the crystal lattice (Li and Hitch 2017), and changes in the microstructure can be analyzed according to the number and location of absorption bands (Xu et al. 2017). The basic spectra were characterized by the absorption bands of Si–O stretching vibration, Si–O–Si stretching vibration, and Si–O–Si bending vibration at  $1000\text{--}1200 \text{ cm}^{-1}$ ,  $600\text{--}800 \text{ cm}^{-1}$ , and  $400\text{--}600 \text{ cm}^{-1}$ , respectively (Chen et al. 2022a, 2022b).

As shown in Fig. 12, after grinding, the Si–O stretching vibration absorption bands quickly degenerated and widened, indicating that grinding destroyed the Si–O bond

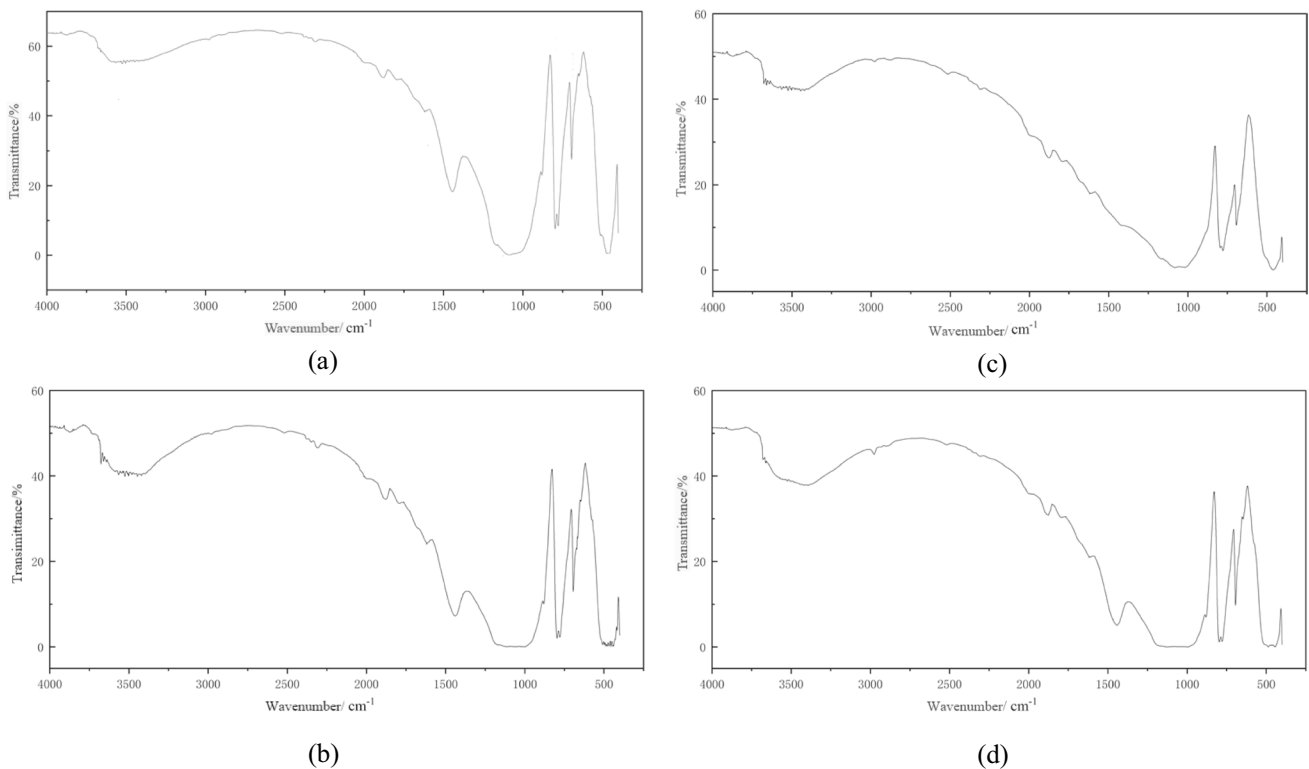


**Fig. 12** Infrared spectra with different grinding times. **a** Grinding 0 h. **b** Grinding 2 h. **c** Grinding 2.5 h. **d** Grinding 3 h. **e** Grinding 3.5 h. **f** Grinding 4 h. **g** Grinding 4.5 h. **h** Grinding 5 h. **i** Grinding 7 h

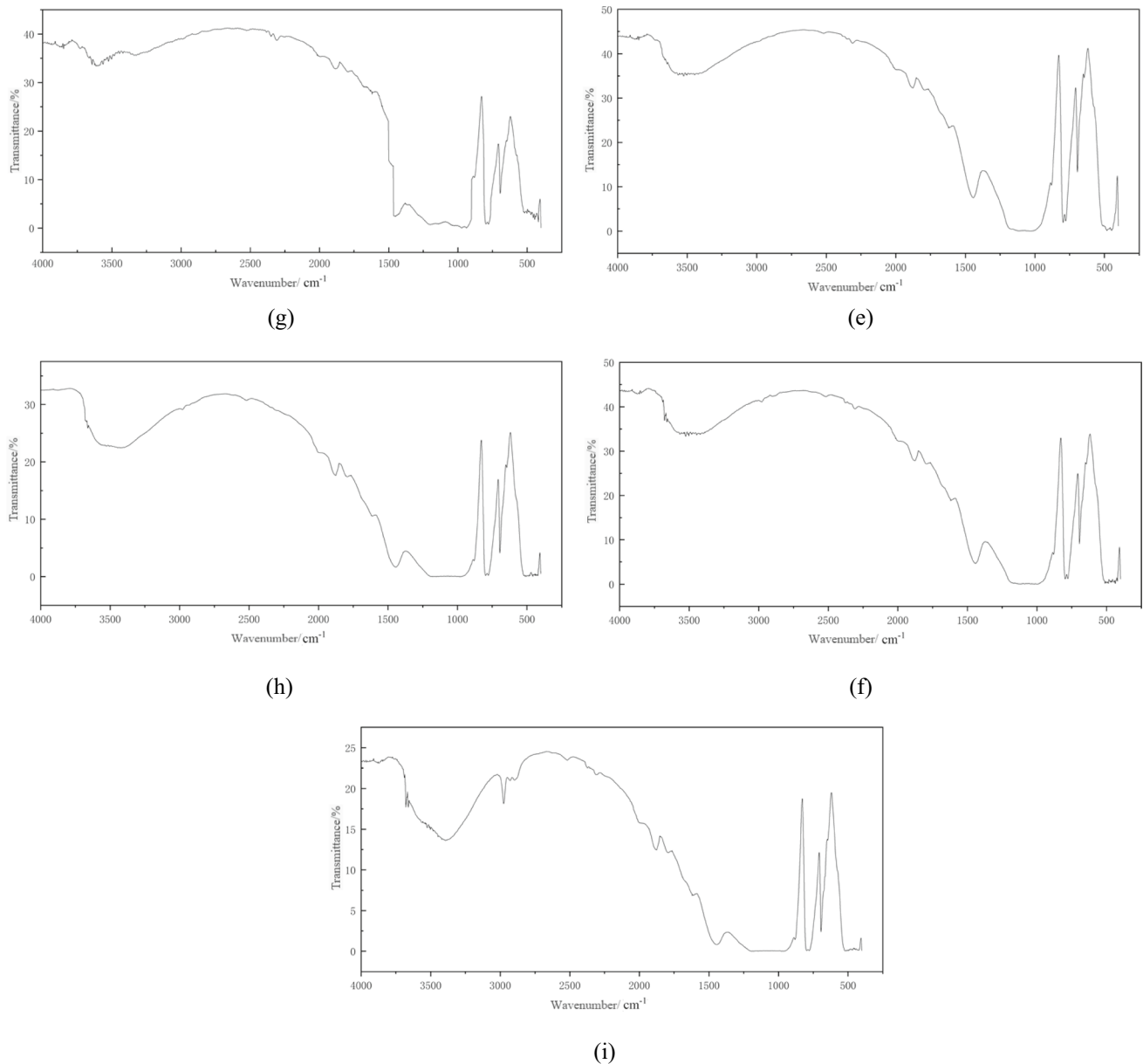


**Fig. 12** (continued)

(Chen et al. 2022a, 2022b) and the order, integrity, and symmetry of the crystal structure were destroyed, as well. The transformation from crystalline to amorphous occurred (Li and Hitch 2017; Wei et al. 2017).

During the milling process, the Si-O bond was cut-off first, and the unsaturated valence bond on the crushed section may have caused recombination and polymerization to form O-Si-O or Si-O-Si, which would restore the symmetry to a certain extent, resulting in a slight increase in the intensity of the symmetric stretching vibration absorption bands. The bending vibration absorption bands were split and sharp, demonstrating that the vibrational activity of the

refined grains was enhanced (Fig. 11), and the enhanced vibration led to the splitting of the peak (Hao 2001).

The analysis results of the infrared spectra further indicated that grinding changed the crystal structure of the main minerals of HSITs, and this was confirmed by the XRD analysis results.

### DSC-TG results and analysis

The DSC-TG curves are shown in Fig. 13.

As shown in Fig. 13, a more obvious exothermic peak appears on the DSC curve after grinding, which is due to the appearance of amorphous state caused by grinding, and

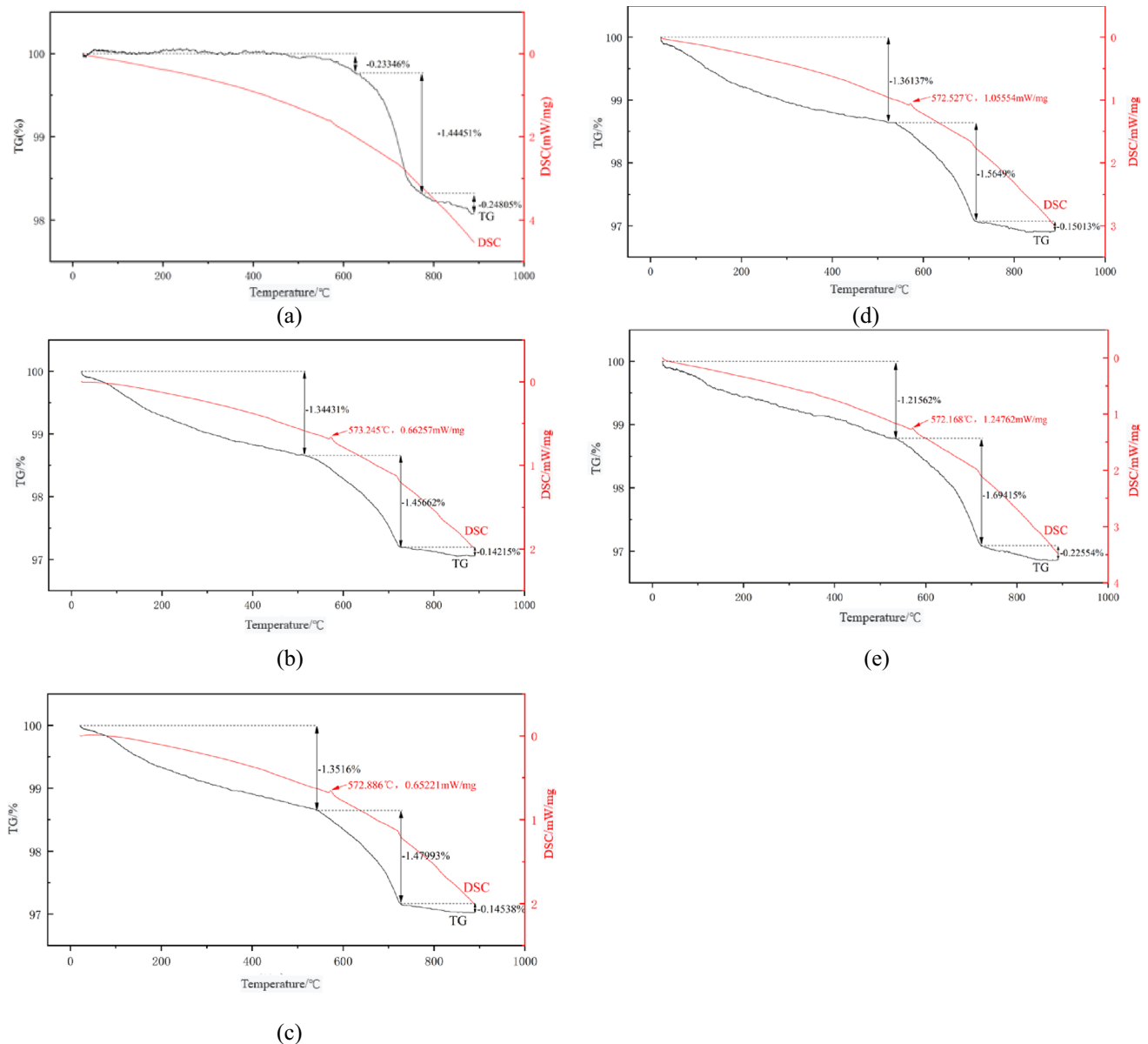


**Fig. 13** DSC-TG curves with different grinding times. **a** Grinding 0 h. **b** Grinding 2 h. **c** Grinding 2.5 h. **d** Grinding 3 h. **e** Grinding 3.5 h. **f** Grinding 4 h. **g** Grinding 4.5 h. **h** Grinding 5 h. **i** Grinding 7 h

the amorphous crystallization releases heat (Wen and Lu 2006). At the same time, it is observed that the exothermic peak gradually shifts to a low temperature, which can be attributed to the reduction in heat required for structures destroyed by mechanical grinding (Sahraoui et al. 2016).

In the TG curve of the ground sample, an obvious weight loss process appears at a lower temperature (200–400 °C). The mass changes with different grinding times when the temperature rises to 900 °C are listed in Table 7.

Table 7 indicates that with the extension of grinding time, the mass change increases, demonstrating that the chemical reaction of ground HSITs is easier to carry out (Vargas and Lopez 2018), and the reaction degree increases with the grinding intensity. This is attributed to the lattice distortion, structural disorder, and the formation of an amorphous layer at the surface of the minerals caused by the mechanical force, which has been confirmed by the aforementioned XRD and FT-IR test results. Thus, the DSC-TG analysis and the thermal behavior verified

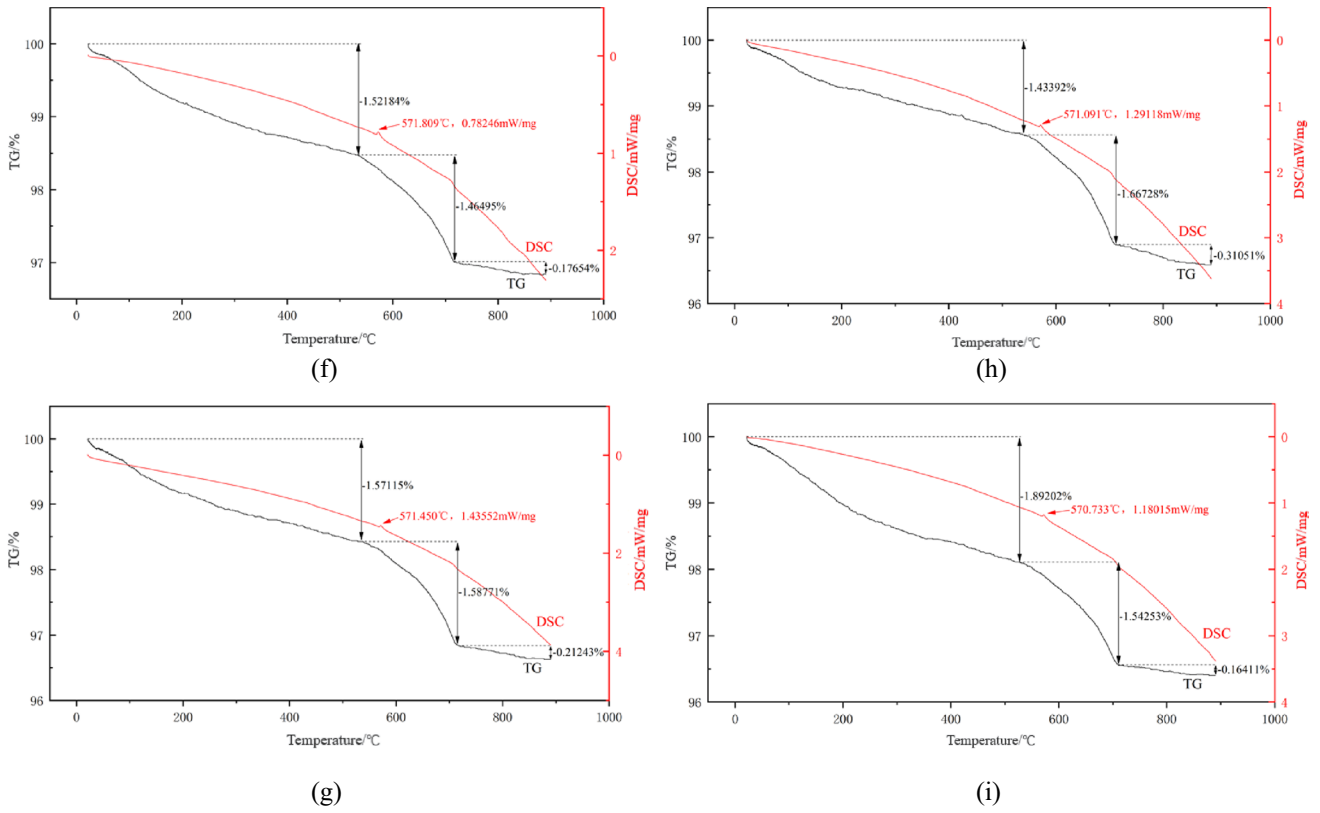


Fig. 13 (continued)

Table 7 Mass loss under different grinding times

Grinding time/h	0	2	2.5	3	3.5	4	4.5	5	7
Mass loss/%	1.92602	2.94308	2.97691	3.07640	3.13531	3.16333	3.37129	3.41171	3.59866

Table 8 Main constituents of cement

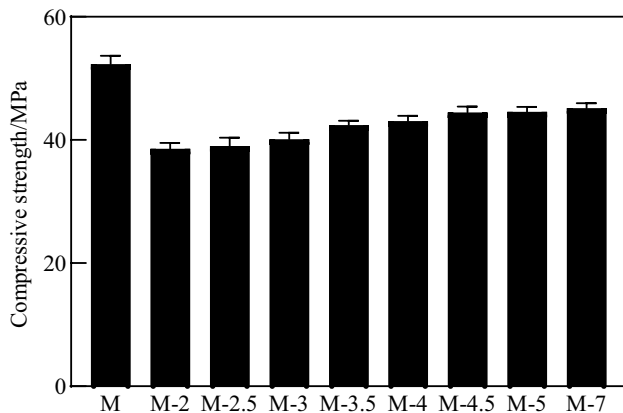
Main chemical constituents/%							Main mineral constituents/%			
CaO	SiO <sub>2</sub>	Al <sub>2</sub> O <sub>3</sub>	Fe <sub>2</sub> O <sub>3</sub>	MgO	SO <sub>3</sub>	LOI	C <sub>3</sub> S	C <sub>2</sub> S	C <sub>3</sub> A	C <sub>4</sub> AF
64.12	20.97	5.10	3.65	3.02	0.91	1.69	51	21.4	9	11

Table 9 Main technical indicators of cement

Setting time/min		Soundness	Compressive strength/MPa		Flexural strength/MPa	
Initial	Final		3 d	28 d	3 d	28 d
135	190	Qualified	27.4	50.5	5.6	8.7

**Table 10** Mortar mix ratio

	Cement/g	Sand/g	HSIT powder/g	Water/ml
M	450 ± 2	1350 ± 5	0	225 ± 1
M-2, M-2.5, M-3, M-3.5, M-4, M-4.5, M-5, M-7	315 ± 2	1350 ± 5	135 ± 2	225 ± 1

**Fig. 14** Compressive strength of the mortar (error bars indicate mean values with standard error of the mean, which were calculated using GraphPad Prism 8.3.0.)

that the mechanical force caused a change in the crystal structure of the main minerals of the HSITs.

### Compressive strength of the cement-HSIT powder composite mortar

Cement-HSIT powder composite mortars were prepared, in which the HSIT powder content was 30%. The mortar compressive strength test was conducted according to the National Standard of the People's Republic of China *Method of testing cements-Determination of Strength* (GB/T17617-1999).

## Materials and mortar mix ratio

### Raw materials

- (1) Cement: ordinary Portland cement with a strength grade of 42.5; its main components and technical indicators are listed in Tables 8 and 9.
- (2) Aggregate: standard sand that meets the national standard of the People's Republic of China *China ISO Standard Sand* (GSB08-1337-2001).
- (3) Iron tailings powder: made by grinding HSITs (described in the second section) for 2, 2.5, 3, 3.5, 4, 4.5, 5, and 7 h.
- (4) Water: drinking water.

### Mix ratios of mortar

The mortar mix ratios are listed in Table 10.

In Table 10, M represents cement mortar; M-2, M-2.5, M-3, M-3.5, M-4, M-4.5, M-5, and M-7 represent mortars mixed with 30% HSIT powder, where the corresponding grinding times are 2, 2.5, 3, 3.5, 4, 4.5, 5, and 7 h, respectively.

## Results and discussion

Figure 14 shows the compressive strength of the mortar. According to the figure, the incorporation of HSIT powder reduces the mortar strength, which changes with the grinding time. The compressive strength shows an upward trend, rising faster before 3.5 h and slower after 3.5 h, which is similar to other performance changes discussed in this paper. In addition, it reflects the existence of a grinding limit of 3.5 h.

Refer to National Standard of the People's Republic of China *Technical Code for application of mineral Admixture* (GB/T51003-2014) to calculate the activity index of HSIT powder, that is, the ratio of the compressive strength of the mortar mixed with 30% HSIT powder to the compressive strength of the control mortar; the activity indexes are shown in Table 11.

The People's Republic of China ferrous metallurgy industry standard *Iron Tailings Powder Used for Cement and Concrete* (YB/T4561-2016) stipulates that the activity index of the iron

**Table 11** Activity index of the HSIT powder

M-2	M-2.5	M-3	M-3.5	M-4	M-4.5	M-5	M-7
0.7374	0.7457	0.7671	0.8108	0.8231	0.8505	0.8515	0.8630

tailings powder used in cement and concrete should be greater than or equal to 0.6. Table 11 shows that all activity indices are greater than 0.6; therefore, the activity of the ground HSIT powder in this study meets the specifying.

In this study, the SiO<sub>2</sub> content of the HSITs was 78.69%. This meets the requirement of the SiO<sub>2</sub> content (not less than 60%) of the iron tailing powder used in cement and concrete stipulated by YB/T4561-2016. As a mineral admixture for CBMs, iron tailing powders should exhibit particle filling and pozzolanic activity. The study has confirmed that the particle size of HSITs after grinding is greatly reduced and smaller than that of cement particles. Therefore, it has good filling performance; at the same time, grinding weakens the crystallization degree of quartz, the main mineral in the HSITs, making it partly amorphous and thus improving the reactivity of HSITs (Zhang et al. 2021).

## Conclusions

The study shows that mechanical force changes the physical and chemical properties of HSITs and changes the crystal structure of their main minerals to a certain extent, thus improving the reactivity. The major conclusions are as follows:

- (1) Grinding improves the particle size distribution of HSITs and increases their specific surface area; grinding decreases the density and increases the solubility of HSITs.
- (2) Grinding reduces the degree of crystallization of the minerals in HSITs and increases the microscopic strain and disorder of the crystal structure.
- (3) The chemical reaction of the ground HSITs proceeds more easily, and the activity index of the HSIT powder is higher than 0.6.
- (4) The grinding limits of the HSITs were determined as 3.5 h.

**Author contribution** Conceptualization, Yun-hong Cheng; methodology, Yun-hong Cheng and Bai-qiang Tong; formal analysis and investigation, Yun-hong Cheng, Bai-qiang Tong, Xiao-hui Sun, and Jing-yu Zhang; writing — original draft preparation, Yun-hong Cheng; writing — review and editing, Yun-hong Cheng; funding acquisition, Yun-hong Cheng; resources, Bai-qiang Tong, Xiao-hui Sun, Jing-yu Zhang; supervision, Yun-hong Cheng.

**Funding** This work was supported by the National Natural Science Foundation of China (Grant No. 51874076)

**Data Availability** The datasets used and/or analyzed during the current study are available from the corresponding author on reasonable request.

## Declarations

**Ethics approval** Not applicable.

**Consent to participate** Not applicable.

**Consent for publication** Not applicable.

**Competing interests** The authors declare no competing interests.

## References

- Akinyemi BA, Alabab PA, Rashedi A (2022) Selected performance of alkali-activated mine tailings as cementitious composites: a review. *Journal of Building Engineering* 50
- Alex TC, Rakesh Kumar SK, Roy SPM (2014) Mechanically induced reactivity of gibbsite: part 1. Planetary milling. *Powder Technol* 264:105–113
- Allahverdi A, Mahinroosta M (2013) Mechanical activation of chemically activated high phosphorous slag content cement. *Powder Technol* 245:182–188
- Boldyrev VV (2006) Mechanochemistry and mechanical activation of solids. *Russian Chem Rev* 75(3):177–189
- Chen Z, Shengyong L, Tang M, Ding J, Buekens A, Yang J, Qiu Q, Yan J (2019) Mechanical activation of fly ash from MSWI for utilization in cementitious materials. *Waste Manage* 88:182–190
- Chen B, Pang L, Zhou Z, Chang Q, Peng F (2022) Study on the activation mechanism and hydration properties of gold tailings activated by mechanical-chemical-thermal coupling. *J Build Eng* 48
- Chen X, Zhang D, Cheng S, Xiong X, Zhao C, Wang X, Qiaoyun W, Bai X (2022) Sustainable reuse of ceramic waste powder as a supplementary cementitious material in recycled aggregate concrete: mechanical properties, durability and microstructure assessment. *J Build Eng* 52
- Cheng Y, Huang F, Li R, Li G, Wei J (2016) Test research on the effects of mechanochemically activated iron tailings on the compressive strength of concrete. *Construct Build Mater* 118:164–170
- Cheng Y, Huang F, Qi S, Li W, Li R, Li G (2020) Durability of concrete incorporated with siliceous iron tailings. *Construct Build Mater* 242
- Cheng Y-h, Yang S-h, Zang J-y, Sun X-h (2022) Test research on hydration process of cement-iron tailings powder composite cementitious materials. *Powder Technol* 399
- de Magalhaes LF, França S, dos Santos Oliveira a M, Peixoto RAF, Bessa c SAL, da Silva Bezerra AC (2020) Iron ore tailings as a supplementary cementitious material in the production of pigmented cements. *J Clean Prod* 274:123260
- Ermolovich EA, Ermolovich OV (2016) Effects of mechanical activation on the structural changes and microstructural characteristics of the components of ferruginous quartzite beneficiation tailings. *Intl J Mining Sci Technol* 26:1043–1049
- Ferreiro S, Frías M, Vigil de la Villa R, Sánchez de Rojas MI (2013) The influence of thermal activation of art paper sludge on the technical properties of blended Portland cements. *Cement Concrete Compos* 37:136–142
- Han F, Luo A, Liu J, Zhang Z (2020) Properties of high-volume iron tailing powder concrete under different curing conditions. *Construct Build Mater* 241
- Han F, Zhang H, Liu J, Song S (2022) Influence of iron tailing powder on properties of concrete with fly ash. *Powder Technol* 398

- Hao B-h (2001) IR analysis of the chemical bond changes in quartz powder during superfine milling. *Mining Metall Eng* 21(2001-04):64–66 (in Chinese)
- Jiang S, Chen T, Zhang J, Duan LX, Yan B (2022) Roasted modified lead-zinc tailings using alkali as activator and its mitigation of Cd contaminated: characteristics and mechanisms. *Chemosphere* 297:134029
- Kitamura M, Senna M (2001) Electrorheological properties of mechanically activated gibbsite. *Intl J Inorg Mater* 3:563–567
- Kiventera J, Lancellotti I, Catauro M, Poggetto FD, Leonelli C, Illikainen M (2018) Alkali activation as new option for gold mine tailings inertization. *J Clean Prod* 187:76e84
- Li J, Hitch M (2017) Structural and chemical changes in mine waste mechanically-activated in various milling environments. *Powder Technol* 308:13–19
- Li J, Ni W, Wang X, Zhu S, Wei X, Jiang F, Zeng H, Hitch M (2022) Mechanical activation of medium basicity steel slag under dry condition for carbonation curing. *J Build Eng* 50
- Lv X, Lin Y, Chen X, Shi Y, Liang R, Wang R, Peng Z (2021) Environmental impact, durability performance, and interfacial transition zone of iron ore tailings utilized as dam concrete aggregates. *J Clean Prod* 292
- Lv Z, Jiang A, Liang B (2022) Development of eco-efficiency concrete containing diatomite and iron ore tailings: mechanical properties and strength prediction using deep learning. *Construct Build Mater* 327
- Perumal P, Niu H, Kiventera J, Kinnunen P, Illikainen M (2020) Upcycling of mechanically treated silicate mine tailings as alkali activated binders. *Minerals Eng* 158
- Perumal P, Kiventerä J, Illikainen M (2021) Influence of alkali source on properties of alkali activated silicate tailings. *Mater Chem Phys* 271:12493213
- Pourghahramani P, Pålson B, Forssberg E (2008) Multivariate projection and analysis of microstructural characteristics of mechanically activated hematite in different grinding mills. *Intl J Mineral Process* 87:73–82
- Purushotham E, Gopi N (2014) Krishna. Effect of particle size and lattice strain on Debye–Waller factors of Fe<sub>3</sub>C nanoparticles. *Bull Mater Sci* 37:773–778
- Purushotham E, Krishna NG (2015) X-Ray Determination of crystal size and effect of lattice strain on the Debye-Waller Factors of Ni nano powders using high energy ball mill. *Chemistry and Materials Research* 7(2015-02) 1-6
- Saedi A, Jamshidi-Zanjani A, Darban AK (2020) A review on different methods of activating tailings to improve their cementitious property as cemented paste and reusability. *J Environ Manage* 270
- Sahraoui T, Belhouchet H, Heraiz M, Brihi N, Guermat A (2016) The effects of mechanical activation on the sintering of mullite produced from kaolin and aluminum powder. *Ceram Intl* 42:12185–12193
- Sajedi F (2012) Mechanical activation of cement–slag mortars. *Construct Build Mater* 26:41–48
- Sajedi F, Razak HA (2011) Effects of thermal and mechanical activation methods on compressive strength of ordinary Portland cement–slag mortar. *Mater Design* 32:984–995
- Sasikumar C, Srikanth S, Mukhopadhyay NK, Mehrotra SP (2009) Energetics of mechanical activation–application to ilmenite. *Minerals Eng* 22:572–574
- Souri A, Golestani-Fard F, Naghizadeh R, Veisesh S (2015) An investigation on pozzolanic activity of Iranian kaolins obtained by thermal treatment. *Appl Clay Sci* 103:34–39
- Tönsuaadu K, Kaljuvee T, Petkova V, Traksmäa R, Bender V, Kirsimäe K (2011) *Intl J Mineral Process* 100:104–109
- Tushar Q, Bhuiyan MA, Zhang G, Maqsood T (2022) Tamina Tamin. Application of a harmonized life cycle assessment method for supplementary cementitious materials in structural concrete. *Construct Build Mater* 316
- Vargas F, Lopez M (2018) Development of a new supplementary cementitious material from the activation of copper tailings: mechanical performance and analysis of factors. *J Clean Prod* 182:427–436
- Wang Z, Chu H, Wang J, Feng E, Zhang Y, Lyu X (2022) Mechanical activation of siliceous tailings and its application as cement admixtures. *Minerals Eng* 177
- Wei B, Zhang Y, Bao S (2017) Preparation of geopolymers from vanadium tailings by mechanical activation. *Construct Build Mater* 145:236–242
- Wen B-J, Lu L (2006) Study of mechanochemistry activate the steel slag. *Bull Chin Ceram Soc* 25(2006-04):89-92+136 (in Chinese)
- Wu R, Liu J (2018). Experimental study on the concrete with compound. Admixture of iron tailings and slag powder under low cement clinker system. *Adv Mater Sci Eng* 9816923
- Wu C-R, Hong Z-Q, Yin Y-H, Kou S-C (2020) Mechanical activated waste magnetite tailing as pozzolanic material substitute for cement in the preparation of cement products. *Construct Build Mater* 252
- Xu Y, Jiang T, Zhou M, Wen J, Chen W, Xue X (2017) Effects of mechanical activation on physicochemical properties and alkaline leaching of boron concentrate. *Hydrometallurgy* 173:32–34
- Yang H, Zhao S, Wang G, Zhang Q, Jin Z, Tong L, Chen G, Qiu X (2022) Mechanical activation modes of chalcopyrite concentrate and relationship between microstructure and leaching efficiency. *Hydrometallurgy* 207
- Yao G, Wang Q, Wang Z, Wang J, Lyu X (2020) Activation of hydration properties of iron ore tailings and their application as supplementary cementitious materials in cement. *Powder Technol* 360:863–871
- Yu R, Dong E, Shui Z, Qian D, Fan D, Wang J, Leng Y, Liu K, Chen Z (2022) Advanced utilization of molybdenum tailings in producing ultra high-performance composites based on a green activation strategy. *Construct Build Mater* 330
- Zhang W, Gu X, Qiu J, Liu J, Zhao Y, Li X (2020) Effects of iron ore tailings on the compressive strength and permeability of ultra-high performance concrete. *Construct Build Mater* 260
- Zhang Z, Zhang Z, Yin S, Linwen Y (2020) Utilization of iron tailings sand as an environmentally friendly alternative to natural river sand in high-strength concrete: shrinkage characterization and mitigation strategies. *Materials* 13:5614
- Zhang N, Tang B, Liu X (2021) Cementitious activity of iron ore tailing and its utilization in cementitious materials, bricks and concrete. *Construct Build Mater* 288
- Zhang M, Li K, Ni W, Zhang S, Liu Z, Wang K, Wei X, Yang Y (2022) Preparation of mine backfilling from steel slag-based non-clinker combined with ultra-fine tailing. *Construct Build Mater* 320
- Zhang N, Hedayat A, Figuero L, Steirer KX, Li H, Sosa HGB, Bernal RPH, Tupa N, Morales IY, Loza RSC (2022) Experimental studies on the durability and leaching properties of alkali-activated tailings subjected to different environmental conditions. *Cement Concrete Compos* 130:104531
- Zielinski PA, Van Neste A, Akolekar DB, Kaliaguine S (1995) Effect of high-energy ball milling on the structural stability, surface and catalytic properties of small-, medium- and large-pore zeolites. *Microporous Mater* 5:123–133

**Publisher's note** Springer Nature remains neutral with regard to jurisdictional claims in published maps and institutional affiliations.